JOURNAL OF MATERIALS SCIENCE **39** (2004) 7161–7168

A demonstration of melt rate control during VAR of "Cracked" electrodes

R. L. WILLIAMSON
Liquid Metals Processing Laboratory, Sandia National Laboratories, Albuquerque, NM 87185-1134, USA
E-mail: rodwill@sandia.gov

J. J. BEAMAN
Mechanical Engineering Department, University of Texas, Austin, TX 78712, USA

D. K. MELGAARD, G. J. SHELMIDINE
Liquid Metals Processing Laboratory, Sandia National Laboratories, Albuquerque, NM 87185-1134, USA

A. D. PATEL, C. B. ADASCZIK
Carpenter Technology Corporation, Reading, PA 19601, USA

A particularly challenging problem associated with vacuum arc remelting occurs when trying to maintain accurate control of electrode melt rate as the melt zone passes through a transverse crack in the electrode. As the melt zone approaches the crack, poor heat conduction across the crack drives the local temperature in the electrode tip above its steady-state value, causing the controller to cut back on melting current in response to an increase in melting efficiency. The difficulty arises when the melt zone passes through the crack and encounters the relatively cold metal on the other side, giving rise to an abrupt drop in melt rate. This extremely dynamic melting situation is very difficult to handle using standard load-cell based melt rate control, resulting in large melt rate excursions. We have designed and tested a new generation melt rate controller that is capable of controlling melt rate through crack events. The controller is designed around an accurate dynamic melting model that uses four process variables: electrode tip thermal boundary layer, electrode gap, electrode mass and melting efficiency. Tests, jointly sponsored by the Specialty Metals Processing Consortium and Sandia National Laboratories, were performed at Carpenter Technology Corporation wherein two 0.43 m diameter Pyromet® 718 electrodes were melted into 0.51 m diameter ingots. Each electrode was cut approximately halfway through its diameter with an abrasive saw to simulate an electrode crack. Relatively accurate melt rate control through the cuts was demonstrated despite the observation of severe arc disturbances and loss of electrode gap control. Subsequent to remelting, one ingot was sectioned in the "as cast" condition, whereas the other was forged to 0.20 m diameter billet. Macrostructural characterization showed solidification white spots in regions affected by the cut in the electrode.

1. Introduction

Vacuum arc remelting (VAR) is a common process used throughout the specialty metals industry for controlled casting of segregation sensitive and reactive metal alloy ingots. In the VAR process, a cylindrically shaped, alloy electrode is loaded into the water-cooled, copper crucible of a VAR furnace, the furnace is evacuated, and a dc arc is struck between the electrode (cathode) and some start material (e.g., metal chips) at the bottom of the crucible (anode). The arc heats both the start material and the electrode tip, eventually melting both. As the electrode tip is melted away, molten metal drips off and an ingot forms in the copper crucible. Because the crucible diameter is larger than the electrode diameter, the electrode must be translated downward toward the anode pool to keep the mean distance between the electrode tip and pool surface constant. This mean distance is called the electrode gap. The objective of VAR is to produce an ingot that is free of macrosegregation, porosity, shrinkage cavities, or any other defects associated with uncontrolled solidification during casting.

In normal industrial practice, several process variables are monitored and recorded to evaluate the status of the VAR process. These include arc voltage (V), melting current (I), electrode position (X), drip-short frequency (f_{DS}) [1], furnace pressure (P), and electrode mass (M). This last process variable is used to estimate electrode melt rate ($\dot{M}$), and modern melt rate

controllers use these estimates as feedback. However, because of the noise inherent in unfiltered load cell data, simply differentiating the output to obtain an "instantaneous" estimate of melt rate yields extremely noisy results. To address this problem, the data are usually filtered, buffered and fit using a running linear least squares regression, the resulting slope being used as the average melt rate over the analysis time. It is not uncommon to use a window that is 10–20 min wide for this analysis, yielding melt rate estimates that lag the VAR process time by 5–10 min. Controllers using these estimates do not work under highly dynamic process conditions where it is necessary to control on a time scale shorter than, or commensurate with, the time over which the load cell data are buffered and analyzed.

Under steady-state conditions, applying constant melting power produces a constant melt rate. However, the simple relationship between power and melt rate under steady-state conditions is destroyed by transients in the electrode temperature distribution. Such transients occur at the beginning and end of normal melting. They may also be caused by common process upsets, such as pressure fluctuations from electrode contamination. Another extremely transient situation arises as the melt zone approaches a transverse crack in the electrode. The crack impedes heat flow causing material below the crack to heat up more rapidly than normal while material above the crack remains relatively cold. Under constant power conditions, this leads to an increase in melt rate as the melt zone approaches the crack, followed by a rapid decrease as the melt zone passes through the crack. Crack-initiated melt rate events are very difficult for standard melt rate controllers to handle.

Electrode melt rate is an important parameter in the VAR process. Variations cause transients in the ingot growth rate and mushy zone thermal gradient, a condition conducive to the formation of melt related defects [2]. For example, such transients have been linked to freckle formation [3] in nickel-base superalloys, as well as solidification white spot formation in Alloy 718 [4]. A method of VAR process control capable of controlling melt rate during transient melting and through common melt rate disturbances could lead to significant improvements in product yields as well as reduce the number of melt related defects in segregation sensitive alloys.

This paper describes the implementation and testing of a method of dynamic VAR process control capable of controlling melt rate through crack events [5]. The tests were performed at Carpenter Technology Corporation in Reading, Pennsylvania. A full treatment of the mathematical development underlying the controller has been reported by Beaman *et al.* [6].

2. A method of dynamic melt rate control

There are two independent, active inputs associated with the VAR control problem: melting current and electrode drive velocity ($\dot{X}$). The latter is used to control electrode gap (G), which, in turn, affects process voltage. Current and voltage determine total process power. The control problem under consideration calls for adjusting current and velocity in such a manner as to minimize the melt rate transient associated with a transverse electrode crack.

During a crack-related melt rate transient, the temperature distribution in the electrode tip changes for the reason described above. Because it is impractical to measure the electrode temperature distribution under normal process conditions, these measurements are not available for control feedback. However, a related variable is melting efficiency (μ). This variable changes throughout the crack event and can be used to track it. Our method of control uses melting efficiency as a crack disturbance variable. Under normal, steady-state melting conditions, it is assumed to be constant. Thus, its associated dynamic equation is very simple:

$$\dot{\mu} = 0. \tag{1}$$

Any transient in the process that causes efficiency to change is considered a process upset or disturbance.

The controller makes use of three other process variables to describe the VAR process: G, M and Δ. This last variable is the thermal boundary layer thickness, a measure of the distance from the electrode tip to the point where the axial temperature gradient in the electrode approaches zero. Thus, Δ is a one-dimensional measure of the electrode temperature distribution. Following Reference 6, the dynamic equations associated with these variables are

$$\dot{G} = a\left(-\frac{\alpha_r C_{S\Delta}}{\Delta} + \frac{C_{Sp}\mu\left[V_C I + (R_I + R_G G)I^2\right]}{h_m A_e}\right) - \dot{X} \tag{2}$$

$$\dot{M} = \rho A_e\left(-\frac{\alpha_r C_{S\Delta}}{\Delta} + \frac{C_{Sp}\mu\left[V_C I + (R_I + R_G G)I^2\right]}{h_m A_e}\right) \tag{3}$$

$$\dot{\Delta} = \frac{\alpha_r C_{\Delta\Delta}}{\Delta} - \frac{C_{\Delta p}\mu\left[V_C I + (R_I + R_G G)I^2\right]}{h_m A_e} \tag{4}$$

where α_r is room temperature thermal diffusivity, V_C is the cathode fall voltage [7], A_e is the cross sectional area of the electrode tip, a is defined as $1 - A_e/A_i$ (A_i is the cross sectional area of the ingot), h_m is the volume specific enthalpy at melt temperature, and R_I and R_G are resistance parameters associated with the circuit and electrode gap, respectively [8]. The expression in square brackets defines melting power when multiplied by μ. $C_{\Delta\Delta}$, $C_{\Delta p}$, $C_{S\Delta}$ and C_{Sp} are constants for a given material. Their specific values depend on the latent heat of fusion and sensible superheat, the melt temperature specific enthalpy, and the room and melt temperature thermal conductivities. The property/variable values specific for Alloy 718 that were used for the controller tests described here are listed in Table I. The thermo-physical properties used in the melting dynamics equations were taken from the literature [9].

Equations 1–4 may be linearized and used to define a VAR process estimator as described in Reference 6. The estimator produces estimates for the four state variables of interest: $\hat{\Delta}$, $\hat{G}$, $\hat{M}$, and $\hat{\mu}$ (a "hat" symbol denotes

TABLE I Alloy 718 properties used for the controller tests

Property/Variable	Value
α_r	0.028 cm^2/s
h_m	5038 J/cm^3
$C_{\Delta\Delta}$	33.84
$C_{\Delta p}$	4.093
$C_{S\Delta}$	5.883
C_{Sp}	1.407
V_C	21.2 V
R_I	4.37×10^{-4} ohm
R_G	0.0 ohm/cm

an estimated value). Three of these estimates are then used for feedback control according to

$$\begin{bmatrix} dI \\ d\dot{X} \end{bmatrix} = \mathbf{K_d} d\hat{\mu} + \mathbf{K_r} \begin{bmatrix} dG_{\text{ref}} \\ d\dot{M}_{\text{ref}} \end{bmatrix} - \mathbf{K} \begin{bmatrix} d\hat{\Delta} \\ d\hat{G} \end{bmatrix} \quad (5)$$

where d in front of a variable indicates the *difference* between the dynamic variable and its associated nominal design value, $\mathbf{K}_d$ is the disturbance gain matrix, $\mathbf{K}$ is the feedback gain matrix, and $\mathbf{K}_r$ is the reference gain matrix. These gain matrices were obtained by the method outlined in Reference 6. Nominal values used in the design of the controller were: $\dot{M}_0 = 60$ g/s, $G_0 = 1.0$ cm, $I_0 = 5590$ A, $\dot{X}_0 = 0.0020$ cm/s, $\Delta_0 = 25.2$ cm, $\mu_0 = 0.48$, and $M_0(t) = M(t_0) - \dot{M}_0(t_n - t_0)$. It should be noted that these values were only used to determine the gains for the controller, and that the actual nominal melting parameters may vary somewhat from these values depending on process conditions.

A schematic of the feedback controller is shown in Fig. 1. Note from the figure that only electrode gap, electrode mass and current measurements are used for control purposes.

3. Controller implementation and performance

The melt rate control tests were performed at Carpenter Technology Corporation. However, processing conditions were chosen so as not to reflect proprietary melting practice. Test 1 involved melting a 0.43 m diameter Pyromet® 718 electrode into 0.51 m diameter ingot. To simulate a transverse crack, the test electrode was cut approximately half way through its diameter using an abrasive saw. The cut was about 0.01 m wide, 0.20 m deep and extended 0.58 m along the circumference of the electrode. It was located 1.40 m from the electrode bottom. Test 2 was nearly identical to Test 1. This was done so that one ingot could be sectioned and investigated as cast, and one could be investigated as billet subsequent to forging.

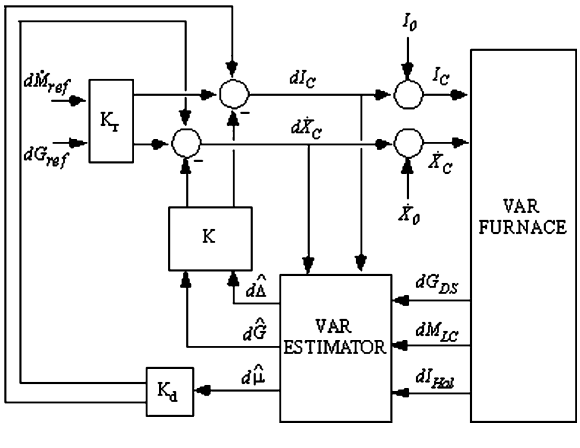

Figure 1 VAR feedback controller schematic. The subscripts on the difference measurements have the following meaning: DS, drip shorts; LC, load cell; Hal, Halmar. These are further discussed in the text.

Measurements of electrode gap, electrode weight and melting current were required as inputs to the estimator. A direct, non-intrusive measurement of electrode gap was not available, so drip-short frequency was measured and the electrode gap calculated according to the following measurement model [10].

$$G_{\text{DS}} = 965.0 f_{\text{DS}}^{-0.595} I^{-0.669}. \quad (6)$$

Electrode weight from load cell tranducers was supplied as an analog signal from the furnace PLC. Current was measured using a Halmar transducer (Model 7ADM, Lem-Dynamp Corp., Grove City, Ohio). All analog signals were read by the control computer (100 MHz 486 PC) using an AT-MIO-16-F5 data I/O card (National Instruments Corp., Austin, Texas) by way of Lem-Dynamp Model MVI isolation amplifiers.

Fig. 2 shows the current and melt rate histories for Test 1. Estimated melt rate clearly follows the reference schedule. Four regions are numbered in the figure: (1) the startup region, (2) the saw cut region, (3) a transient melt rate test, and (4) the hot-top region. The region of interest for this study is Region 2.

Load cell and five-minute "average" melt rate histories from the region where the saw cut was encountered by the melt zone are shown in Fig. 3. As is apparent from the figure, the saw cut gives rise to a small perturbation in the five-minute melt rate. Performance could, no doubt, be improved slightly by controller tuning. However, given the size of the disturbance, the data show that relatively good melt rate control was maintained. Linear regression of the load cell data over the region shown in the figure gives a melt rate of 61.9 g/s with a regression coefficient of 0.99998. As seen from Fig. 2, melting current began to respond to the saw cut some time before the cut was actually encountered. As the melt zone approached the cut, efficiency began to increase causing the current to be cut back. This response began about 40 min before the melt zone reached the cut. When the arc encountered the cold material on the other side of the cut, efficiency suddenly dropped causing a large, rapid increase in melting current.

Drip-short frequency data show that the controller encountered some difficulties in holding gap through the saw cut event. This was expected due to the width of the cut—the estimator becomes confused when it encounters a step in the electrode tip that is the same size as the reference gap itself. Furthermore, there was visual evidence of severe arc disturbances during the event possibly related to electrode material directly under the

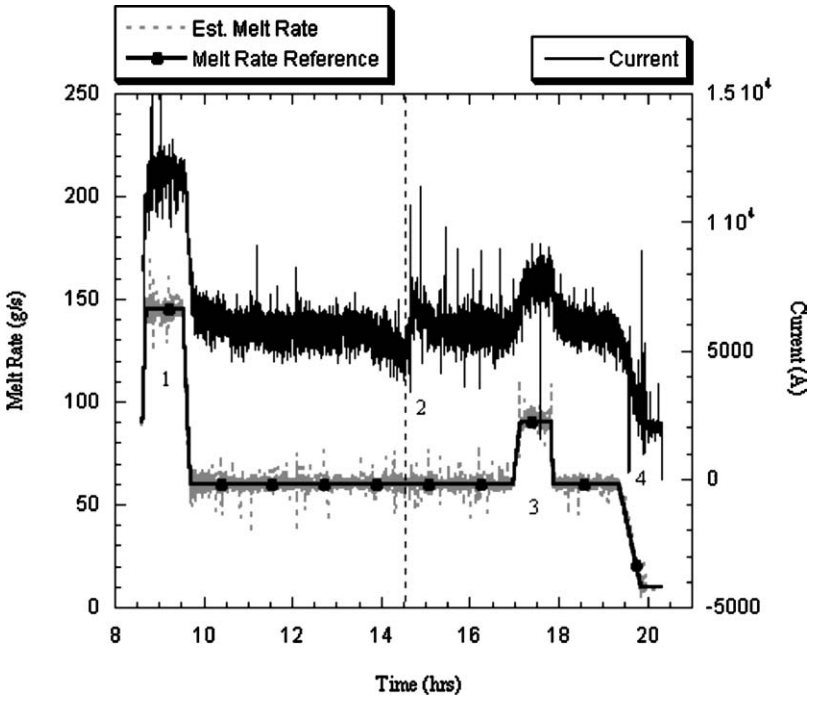

Figure 2 Current and melt rate histories for Test 1. The dashed line marks the approximate time at which the melt zone passed through the saw cut.

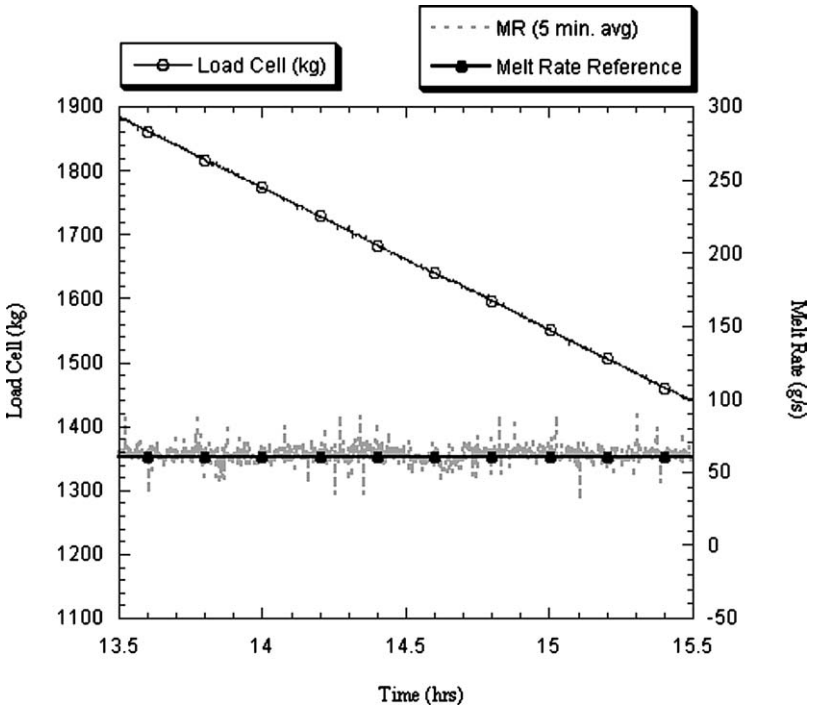

Figure 3 Load cell and melt rate traces from the saw cut region (region 2 in Fig. 2).

cut dropping down and contacting the pool as the arc zone approached. The arc became constricted a number of times and significant shelf growth was observed on one side. Such conditions are clearly outside the range of arc events for which the controller was designed. Still, the controller recovered gap control immediately after the event and melt rate control was stable.

Electrode gap control during steady-state melting was exercised briefly during Test 1. Three electrode gap steps were commanded: from 1.0 to 0.8 cm, from 0.8 to 0.6 cm, and from 0.6 cm back up to 1.0 cm. The objective of the exercise was to test the controller's ability to run at very tight electrode gaps—average drip-short frequency in the range of 15–20 s^{-1}. It was observed that control was maintained at the smallest gap and that the steps were relatively sharp.

4. Ingot and billet results

4.1. Ingot characterization

The total height of the Test 1 ingot was 1.69 m. The startup region was 0.318 m, and the steady-state region was 1.245 m in height. Prior to cutting longitudinal and transverse sections, the ingot was homogenized and this distorted the as-cast grain structure. The ingot was cut

into five pieces from which 1.3 cm thick longitudinal plates were cut with one face containing the ingot axis. The plates were cut in half, ground and conditioned using 80 grit paper. They were then etched in a solution of ferric chloride and photographed.

The ingot macrostructure from the region of the saw cut is shown in Fig. 4. As expected, the center of the ingot has long columnar grains along the vertical axis; the mid-radius region also has columnar grains at about 45^o to the vertical axis. Fine grains characterize the surface. The region from 1.3 to 12.5 cm from the surface shows recrystallization and possibly some grain growth due to the homogenization process. The region corresponding to the saw cut in the electrode shows a fine columnar dendritic structure at the center. The reason for this is not clear. Niobium and molybdenum compositions were measured at several locations in samples taken from the center, mid-radius and surface of the ingot using a spark ablation optical emission spectrometer with a spot diameter of about 6 mm. The data showed no macrosegregation within the measurement accuracy of 0.2 wt %. The melt zone reached the crack in the electrode after nearly six hours of melting (furnace time of 14.6 h), at which time the ingot height was ∼0.91 m. A band of equiaxed grains ∼2 cm thick and located ∼7.5 cm from the bottom of the plate (see Fig. 4) apparently marks the pool location when the crack disturbance was encountered.

4.2. Billet characterization

As mentioned, the VAR melting parameters in the crack region were identical in both test melts. After VAR, Ingot 2 was homogenized and forged to a 0.216 m round billet. After forging, several 1.3 cm thick transverse slices were cut from selected regions. Each slice was macro-etched and subjected to routine macro-inspection. Both axial and radial locations of anomalies were noted. The following relationship was used to relate a particular location in the billet to its corresponding location in the ingot:

$$(r_{\mathrm{b}},\ z_{\mathrm{b}}) = \left(a r_{\mathrm{i}},\ \frac{z_{\mathrm{i}}}{a^2}\right) \tag{7}$$

where $a = 0.425$ is the ratio of the billet to the ingot diameter, r is the radial coordinate and z is the axial coordinate. The subscripts "b" and "i" denote billet and ingot, respectively.

The billet macrostructure revealed numerous solidification white spots, wisps or hook shaped, 1–2 mm in size, about 2.5–6.0 cm from the surface of the forged billet. Micro-probe analysis showed a niobium depletion of 10–15% within the white spots. A complete plot of the white spot location along the ingot is shown in Fig. 5. Essentially, solidification white spots were found in regions subjected to melt rate fluctuations during melting. We note that the melt rate fluctuation in the region of 12.5–13.0 h was due to a procedural error by the operator.

5. Discussion

The results demonstrate the controller's ability to track and automatically compensate for changing thermal conditions in the electrode. However, it should be emphasized that this is accomplished somewhat artificially through the disturbance variable, μ. Certainly, changes in Δ occur in response to changes in μ and corresponding changes in I (see Equation 4). However, the controller attempts to change μ and I in precisely the manner required to hold the melt rate at its reference value, which amounts to holding the *estimated* thermal boundary layer, $\hat{\Delta}$, constant through the disturbance. Indeed, only very small changes in $\hat{\Delta}$ were observed during the disturbance, and then only during the most dynamic part.

As seen from the results, the controller did not respond perfectly to the saw cut, the event being marked by perturbations to melt rate and electrode gap, giving rise to a clear signature in the ingot macrostructure. However, it should be emphasized that a cut of this depth and width constitutes an enormous process disturbance. Using conventional industrial controllers, it is not uncommon to observe excursions as large as 50% in average melt rate when passing through a crack disturbance. Relative to this, the controller's performance through the cuts was quite good, holding average melt rate to within 15% of its reference set-point.

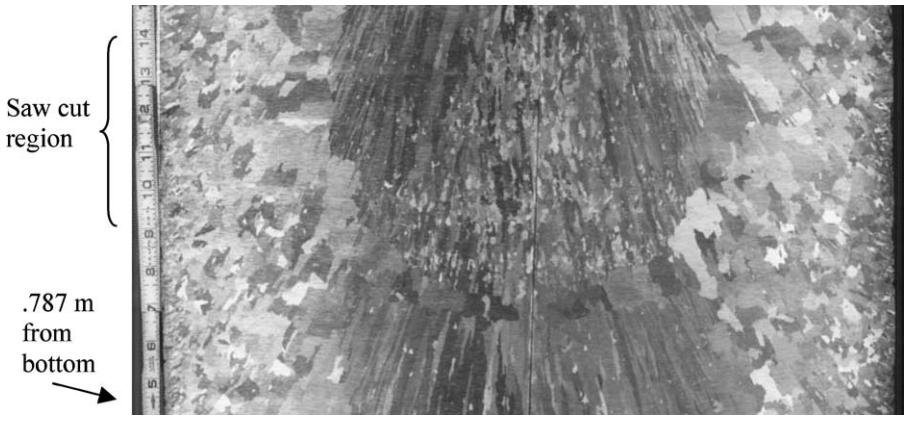

Figure 4 Ingot macrostructure from the saw cut region in the cast ingot. The grain structure due to the cut is apparent in the photo. This slice represents a ingot height of 0.280 and 0.508 m in diameter. It should be noted that the scale in the macrograph is in inches.

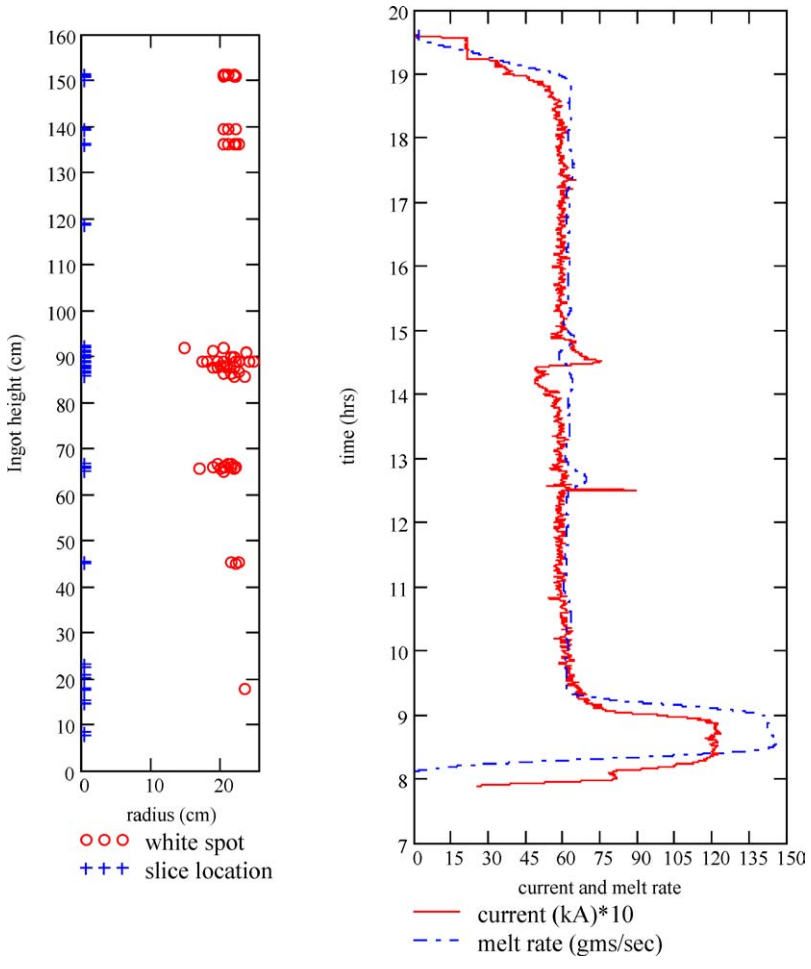

Figure 5 White spot location in Ingot 2. The actual location was measured in the billet and the data was transferred to the ingot using Equation 7. In this figure, the white spots are all shown on one side of the ingot; in reality they were seen at different angular locations in the billet. The location of the slices is indicated by the "+" sign along the left axis. Also shown on the right is the melt rate and current plot for this heat.

BAR [11], a 2-D axi-symmetric ingot casting code, was used to simulate the changes to the pool profile due to the fluctuations in melting current and melt rate as the melt zone progressed through the saw cut region. We emphasize that the simulations only evaluate the effects of melt rate and current excursions on pool profile, and do not address the other issues associated with the cut event such as off-axis power input, material fall-in, arc interruptions, and so forth. Since the melt rate perturbation in the crack region was minimal, the resulting effect on the pool depth is also minimal. As seen in Fig. 6, simulated pool depth increases to 12 cm from its steady-state value of 11.2 cm. This corresponds to an increase in pool depth of about 7% during the melt rate (20 min average) perturbation of ±5%. It should be noted that, although the current varied through a range of ~2000 A in this region, its effect on the pool depth is small since the molten metal flow at these current levels is primarily driven by buoyancy forces. Details of model formulation and validation are in Reference 11.

Equation (3) can be used to calculate melt rate under conditions of constant current using the estimated efficiency from one of the test trials. Fig. 7 shows the resulting melt rate and pool depth from BAR for a constant current simulation. As seen, the constant current simulation predicts a melt rate variation of ± 30% and the pool depth increases from about 11.2 cm just prior to the crack to 13.5 cm just after the melt rate reaches its peak value. This pool depth increase of about 2.3 cm (20%) is significantly larger than that obtained when controlling melt rate. Given this information, it seems reasonable that, under such conditions, constant melt rate control holds some advantage over constant current control with respect to its impact on solidification as long as melting current does not reach a point where magneto-hydrodynamic effects begin to reverse flow in the pool.

Having made this assertion based on simulations, it is still clear from Fig. 5 that the saw cut event produced a great number of solidification white spots even with relatively good melt rate control. However, this may also be attributed to the fact that the event produced arc interruptions and loss of gap control as described above. Furthermore, one must keep in mind that the conditions chosen for these tests do not reflect standard industrial melt practices and have not been chosen to minimize the probability of solidification white spot formation. Thus, solidification white spots were found in several other places in the ingot where small current or melt rate perturbations were introduced to the process. The important point is that a method of model-based melt rate control has been demonstrated that provides a means of achieving highly responsive melt rate control under normal melting conditions as well as under conditions

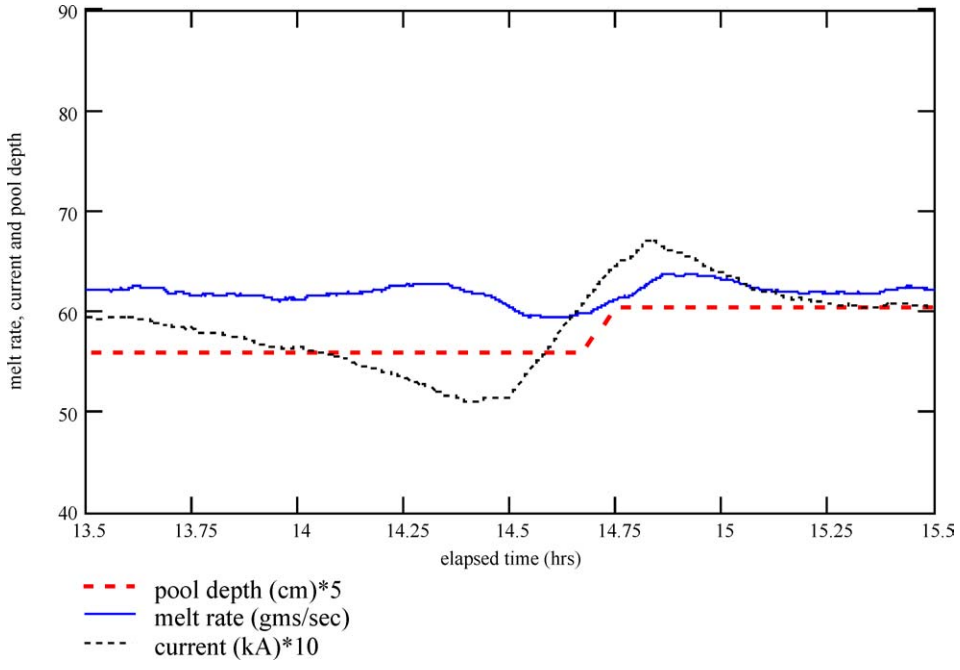

Figure 6 Simulated pool depth response to a current deviation of the same size as that used to control the melt rate through the saw cut disturbance.

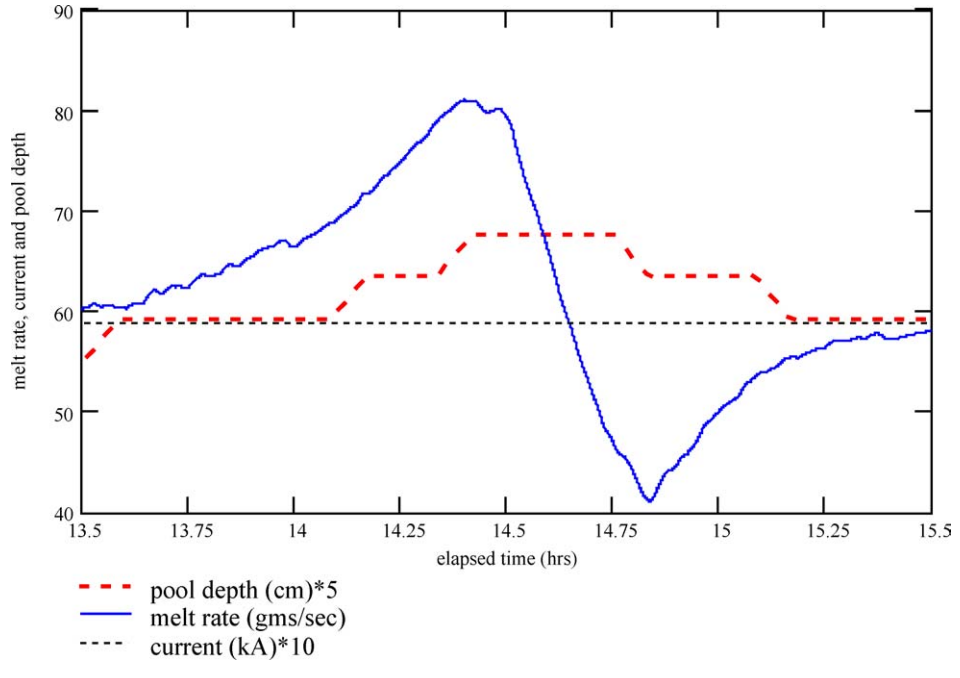

Figure 7 Simulated pool depth response to a melt rate deviation caused by holding current constant and letting the efficiency vary as it did through the saw cut disturbance.

where the electrode temperature distribution has been driven away from, or not yet achieved, steady-state.

6. Conclusions

The following conclusions may be drawn from this work:

1. The model-based VAR process controller developed by Beaman *et al.*[6] is able to maintain relatively good melt rate control through a saw cut disturbance, indicating that this method is also effective at controlling melt rate through a transverse crack disturbance.

2. Electrode gap was not effectively controlled when the melt zone reached the saw cut due to arc interruptions possibly related to material falling off the electrode. Good electrode gap control was maintained at all other times during the test.

3. The cut disturbance produced numerous solidification white spots despite relatively good melt rate control. However, this can be attributed to arc interruptions associated with loss of gap control and material fall-in, as well as the fact that the test melt procedure was not optimized to prevent white spot formation.

4. Based on simulation results reflecting the melt rate and current conditions of these tests, controlling melt rate to a constant reference value is more effective at

minimizing the effects of crack disturbances on pool depth than controlling melting current to a constant reference value.

Acknowledgements

A portion of this work was supported by the United States Department of Energy under Contract DE-AC04-94AL85000. Sandia is a multiprogram laboratory operated by Sandia Corporation, a Lockheed Martin Company, for the United States Department of Energy. Support for this work was also provided by the United States Federal Aviation Administration and the Specialty Metals Processing Consortium. The authors gratefully acknowledge the support and cooperation of Carpenter Technology Corporation, Reading, Pennsylvania, for hosting the tests and providing ingot and billet preparation and analysis. They would especially like to thank Walter Johnson, Robert Morrison, Glenn Troxel, Gregory Miller and all the Operations and Maintenance personnel at Carpenter for their assistance during these trials.

References

1. Drip-shorts are momentary arc interruptions due to metal drips bridging the electrode gap and contacting the ingot pool surface. See F. J. ZANNER, *Metall. Trans.* B, **10B** (1979) 133 for a detailed description of drip-short signatures.
2. M. C. FLEMMINGS, "Solidification Processing" (McGraw-Hill, New York, NY, 1974) p. 245.
3. T. SUZUKI, T. SHIBATA, K. MORITA, T. TAKETSURU, D. G. EVANS and W. YANG, in Proceedings of the 2001 International Symposium on Liquid Metal Processing and Casting, Santa Fe, NM, Sept. 2001, edited by A. Mitchell and J. A. Van Den Avyle (American Vacuum Society, 2001) p. 325.
4. L. A. BERTRAM, J. BROOKS, D. G. EVANS, A. PATEL, J. A. VAN DEN AVYLE and D. D. WEGMAN, in Proceedings of the 1999 International Symposium on Liquid Metal Processing and Casting, Santa Fe, NM, February 1999, edited by A. Mitchell, L. Ridgeway and M. Baldwin (American Vacuum Society, 1999) p. 156.
5. L. A. BERTRAM, R. L. WILLIAMSON, D. K. MELGAARD, J. J. BEAMAN and D. G. EVANS, U.S. Patent 6,115,404, Sept. 5, 2000.
6. J. J. BEAMAN, R. L. WILLIAMSON and D. K. MELGAARD, in Proceedings of the 2001 International Symposium on Liquid Metal Processing and Casting, Santa Fe, NM, Sept. 2001, edited by A. Mitchell and J. A. Van Den Avyle (American Vacuum Society, 2001) p. 161.
7. B. JUTTNER and V. F. PUCHKAREV, in "Handbook of Vacuum Arc Science and Technology", edited by R. L. Boxman, D. M. Sanders and P. J. Martin (Noyes Publications, Park Ridge, NJ, 1995) p. 119.
8. F. J. ZANNER and L. A. BERTRAM, in Proceedings. 8th Conference on Vacuum Metallurgy (1985) p. 512.
9. P. N. QUESTED, K. C. MILLS, R. F. BROOKS, A. P. DAY, R. TAYLOR and H. SZELAKOWSKI, in Proceedings of the 1997 International Symposium on Liquid Metal Processing and Casting, Santa Fe, NM, Feb. 1997, edited by A. Mitchell and P. Aubertin (American Vacuum Society, 1997) p. 1.
10. R. L. WILLIAMSON, F. J. ZANNER and S. M. GROSE, *Met. Mat. Trans.* B **28B** (1997) 841.
11. L. A. BERTRAM, C. B. ADASCZIK, D. G. EVANS, R. S. MINISANDRAM, P. A. SACKINGER, D. D. WEGMAN and R. L. WILLIAMSON, in Proceedings of the 1997 International Symposium on Liquid Metal Processing and Casting, Santa Fe, NM, February 1997, edited by A. Mitchell and P. Aubertin (American Vacuum Society, 1997) p. 110.

Received 10 March
and accepted 11 June 2004